Advancement in Science and Technology Research
Vol. 2(3), pp. 42-53, July 2015
ISSN: 2437-1319
Full Length Research Paper

Simulating the operation of silicon photovoltaic cells at outer space environments

S. M. El-Ghanam[1], W. Abd El-Basit[1] and F. A. S. Soliman[2]*

[1]Electronics Res. Lab., Physics Dept., Faculty of Women for Art, Science, and Education, Ain-Shams Univ., Heliopolis, Cairo, Egypt.
[2]Nuclear Materials Authority, P. O. Box 530, Maadi-11728, Cairo, Egypt.

Accepted 29 June, 2015

ABSTRACT

All solar cells that are developed for use in space must take into consideration the unique aspects of the space environment. The spectral illumination that is available in space is not filtered by our atmosphere and thus is different from what is experienced on Earth. In this concern, a study was conducted to evaluate the performance of silicon photovoltaic systems exposed to isotropic irradiation, protons and electrons, which approximate the space irradiation effects. Also, the study extended to include the operation of such devices at extreme low temperatures down to cryogenic levels. Significant degradation was experienced in the silicon cells output characteristics after bombardment with either protons fluence (10^{14} to 10^{16} p/cm^2) within the energy range from 0.6 to 6.0 MeV or electron fluencies up to 1.0×10^{13} electron/cm^2 at energies up to 12.0 MeV. For low energy protons (from 0.6 MeV to 2.0 MeV), the damage rate per particle decreases as the energy increases. The decrease is approximately inversely proportional to particle energy. At higher energies (up to 6.0 MeV) the damage level is almost constant. Also, for the case of electron irradiation, the damage rate is shown to decrease the open circuit voltage, and the short circuit current. Consequently, this decreases the output power. On the other hand, the short circuit current was shown to be un-sensitive function of temperature, where for the temperature range from +300°C down to -160°C, a rate of current decrease of 6.42 µA/°C was reported. The main variation was observed to be due to open circuit voltage, where for the same temperature range, a rate voltage increase with 1.90 mV/°C was recorded. Finally, the cell output power was shown to increase, within the temperature range, at rate of 15.64 µW/°C.

Keywords: Solar cells, protons, electrons, low temperature, space environment.

*Corresponding author. E-mail: fouad.saad.soliman@gmail.com.

INTRODUCTION

Starting from 1953 when the semiconductor solar cell (SC) was invented, SCs were mainly applied in the space satellite energy systems. Up to 1990 the solar cells were created on the base of single crystal, poly-crystal and amorphous Si mainly caused by the comparatively high efficiency of these solar cells (η = 12 to 17%) and relatively cheap technology (Torchynska, 2004; Gordon, 2015). Up till now Si-SC still provided the power majority for space and eventually the solar arrays for the International Space Station (ISS) and spacecrafts to Mars (Figure 1).

For long duration of spacecraft missions, the high doses of radiation can damage electronic components and solar cells. A major concern is also radiation-induced "single-event effects" such as single event upset (Silverman, 1995; Johnson and Kierein, 1992). Manned missions usually avoid the radiation belts and the international space station is at an altitude well below the most severe regions of the radiation belts. During solar energetic events (solar flares and coronal mass

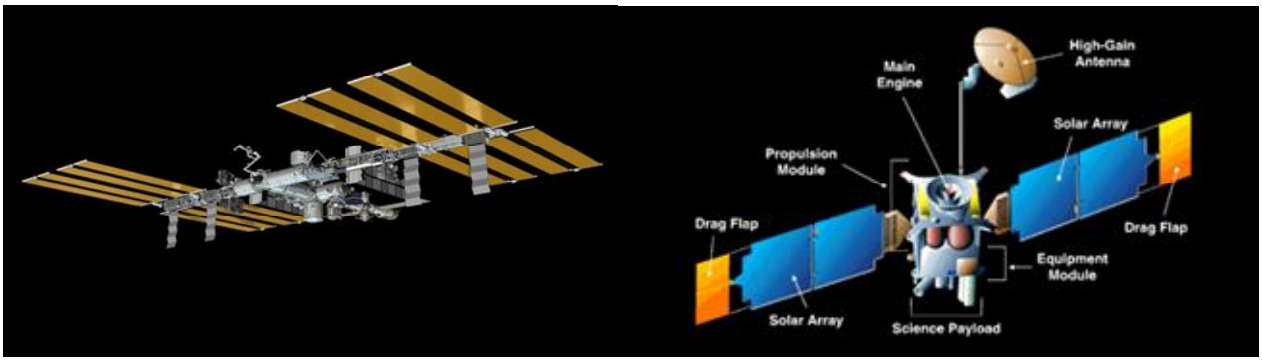

a b

Figure 1. Spacecraft station (a), and spacecraft to Mars (b), by NASA (Adams et al., 1991; Holmes-Siedle and Adams, 2002; Shprits et al., 2008).

ejections) particles can be accelerated to very high energies and can reach the Earth in times as short as 30 min (but usually take some hours). These particles are mainly protons and heavier ions (Figure 2) that can cause radiation damage, disruption to logic circuits and even hazards to astronauts. Manned missions to return to the moon or to travel to Mars will have to deal with the major problems presented by solar particle events to radiation safety, in addition to the important contribution to doses from the low-level background cosmic rays. In near-earth orbits, the earth's geomagnetic field screens spacecraft from a large part of these hazards - a process called geomagnetic shielding (Santina, et.al, 2003; Stassinopoulos, 2003).

Proton belt

The proton belt is located from about 500 km above Earth's surface and extends to 13,000 km (Figure 3a). This Inner Belt contains protons with energies greater than 10 million volts. Scientists currently think that these protons are trapped cosmic ray particles from outside the solar system, or from the sun itself possibly during severe solar flares. Here is what this belt looks like if you were to slice in like a water-melon (Cattell, 2008; NASA, nd; www.astrogle.com/discus/index.php?topic=1092.0).

Electron belt

Low energy electron belt

The low-energy electron belt actually overlaps the volumes of space where the proton belt is located in the Inner Belt (Figure 3b). The electrons carry between 1.0 and 5.0 MV of energy, on average (Earth's Radiation Belts: A Tutorial – ACD).

High-energy electron belt

The high-energy electron belt is located further out than the two over lapping inner belts, and in the above figure it is colored purple. Electrons in this outer belt carry between 10 to 100 MV of energy, on average (Earth's Radiation Belts: A Tutorial – ACD).

Spacecraft electrostatic charging can be caused by the hot plasma environment around the Earth. The plasma encountered in the geostationary orbit region becomes heated during geomagnetic "sub-storms" caused by disturbances in the solar wind. "Hot" electrons (with energies in the keV range) collect on spacecraft surfaces and can establish electrostatic potentials in the order of kilovolts. As a result, discharges can occur and are known to be the source of many spacecraft anomalies.

Solutions devised by scientists and engineers include, but are not limited to, spacecraft shielding, special "hardening" of electronic systems, various collision detection systems. Effects evaluation during spacecraft design includes application of various environment 'models' (Novikov, 2008), including radiation belt models, spacecraft-plasma inter-action models and atmospheric models to predict drag effects encountered in lower orbits and during reentry.

Radiation physics

When high-energy radiation falls on a device, energy is deposited on a semiconductor via two mechanisms; atomic displacement and ionization. The relative importance of these mechanisms in a semiconductor depends on both the radiation type and the device nature. The initially produced defects for electron-irradiation are quite simple and can be expressed as single displaced atom and its associated vacancy [Frankel Defect (Soliman, 1988)]. The interaction is

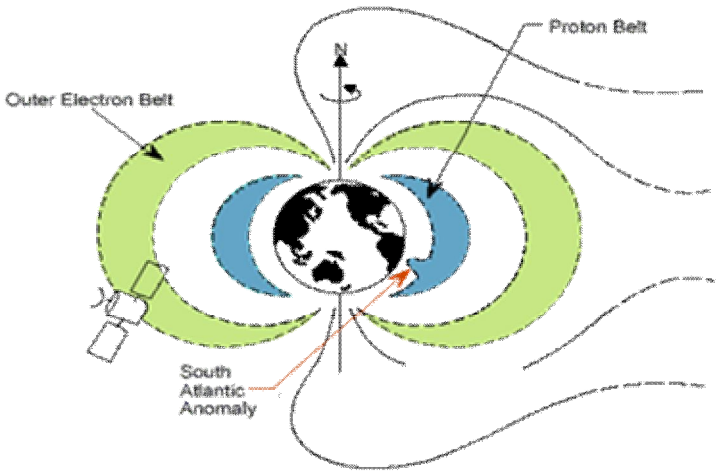

Figure 2. Radiation belt around earth (Adams et al., 1991; Holmes-Siedle, and Adams, 2002; Shprits et al., 2008).

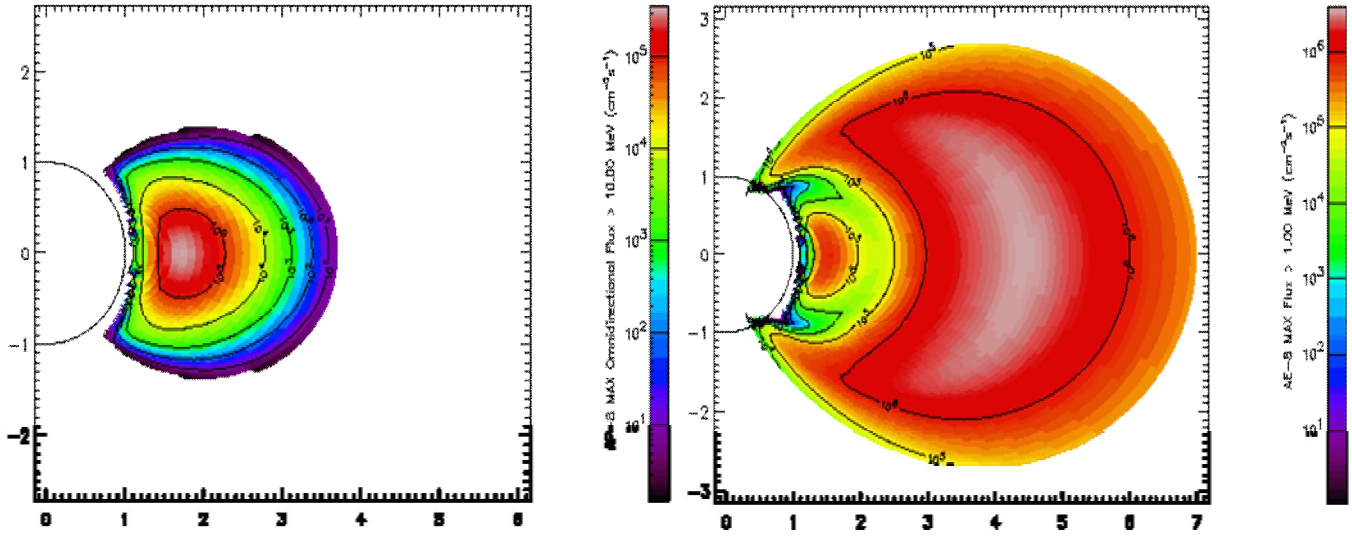

Figure 3. Proton radiation (a), and electrons (b) belts around earth (Earth's Radiation Belts: A Tutorial – ACD; Novikov, 2008; Soliman, 1988).

simply described by the number of defects/cm^2 created, which is given by Marzouk and Soliman (1987):

$$N_t = \Phi . a_d . N_o \quad (1)$$

Where, a_d is displacement cross-section in cm^2, ϕ is radiation fluence, and No is the number of lattice atoms/cm^2.

For calculating the number of detects/cm^2 created due to different radiation types, one may use Figure 4, which shows the displacement cross-section versus radiation energy for silicon crystals. It can be shown that the point defect result in the introduction of allowed energy states within the semiconductor forbidden gap. This energy states lead to the following:

(a) Carrier removal: majority carrier density is reduced by the radiation fluence, and the carrier removal rate is:

$$dn/d\phi = Ao\,[1 - \exp(\zeta_T - \zeta_F) / K_T)] \quad (2)$$

where, Ao is constant, ζ_T is the defect energy, ζ_F is the Fermi level, T is temperature, and K is the Boltzmann's

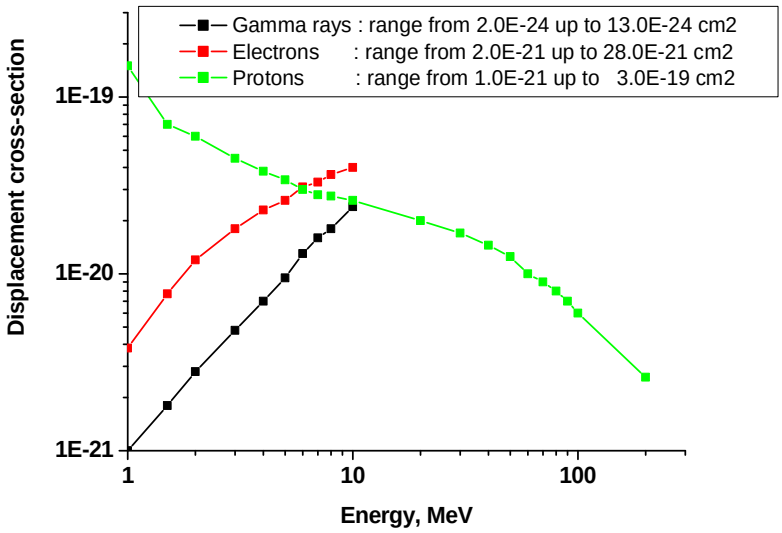

Figure 4. Displacement cross-section versus energy for silicon irradiated with protons, gamma-rays, and electrons, compiled by the authors (Soliman, 1988; Marzouk and Soliman, 1987).

constant.

(b) Mobility degradation: the mobility is shown to decrease with increasing the radiation fluence, and the mobility degradation rate is:

$$d(1/\mu)/d\phi = Ao[1- (\zeta_T - \zeta_F) / KT) (1/B_0)] \quad (3)$$

where, μ is the mobility, and B_0 is constant.

(c) Conductivity modulation: since the carrier concentration and mobility both decrease with radiation, it is obvious that the conductivity will also decrease.
(d) Minority carriers lifetime: degradation rate in minority carrier lifetime is expressed as:

$$d(1/\tau) / d\Phi = K\tau \quad (4)$$

where $K\tau$ is the carrier lifetime damage constant.

Temperature in space

When calculating the temperature in space, it is important to understand that most estimates must take into account the varied space makeup. Outer space is usually considered to be the portion of the universe that is almost entirely empty and, from the Earth point of view, officially begins at an altitude of about 100 kme above sea level. In the void between planets, star systems and galaxies, the temperature in space is generally considered to be 2.725°K which is -270.4°C (Owen et al., 1999). This is only a very small amount above absolute zero, the coldest possible temperature at which the movement of all matter ceases at -273.15°C. Closer to Earth, such as just outside of Pluto's orbit, the temperature is estimated to be closer to 35 or 40°K due to the distance to the Sun effect. This is still very cold, but nowhere near as cold as somewhere in deep space, far from any sunlight. Finally, Table 1 illustrates the operational temperatures for unheated space-craft in the outer planets environments.

Table 1. Operational temperatures for unheated spacecraft in the environments of the outer planets.

Mission	Temperature, °C	Temperature, K
Mars	-20 to -120	253 to 153
Jupiter	-151	122
Saturn	-183	90
Uranus	-209	64
Neptune	-222	51
Pluto	-229	44

EXPERIMENTAL PROCEDURES

For the present investigation, the electrical performance of silicon solar cells set with different dimensions rectangular shapes were tested. The chosen samples were Sargent-Welch fabricated and having the specifications illustrated in Table 2. For all the samples their open circuit voltage, short circuit current, and spectral response were plotted as a functions of

Table 2. Sample specifications for commercial silicon "n/p" type photovoltaic cells [Sargent-Welch, nd].

Catalogue no.	Dimensions, mm	Junction depth, µm	Thickness, µm	Current, mA	Voltage, V	Power, mW
2148	20 × 10	0.6 - 0.8	250 - 300	36.0	0.45	16.0
2148-15	10 × 5	0.6 - 0.8	250 - 300	10.0	0.45	4.60

temperature (in the range from + 300°C down to –160°C), or either protons fluence (10^{14} to 10^{16} p/cm^2) within the energy range from 0.6 to 6.0 MeV or electron fluencies up to 1.0×10^{13} electron/cm^2 at energies up to 12.0 MeV.

Temperature tests

The temperature ranges were taken to be: (a) from -160°C up to room level, and (b) from room level up to +300°C. In this concern, the cooling system shown in Figure 5 was used during the course of the study, where its basic components are: a special glass cell with its glass cover having embedded tungsten electrodes, pressurized gas cylinder and liquid nitrogen Dewar flask (Abdel Basit et al., 2013; El-Ghanam and Abdel Basit, 2011). The glass container was connected to a vacuum system and to the nitrogen gas cylinder via three way T-junction glass valve. The glass cell immersed in the Dewar flask, and the open part of the top of the Dewar flask was covered by thin disc of insulating material for thermal isolation. The glass cell was evacuated by a rotary pump, and hence the dry nitrogen gas was admitted to the cell and its pressure is then adjusted to be slightly higher than the atmospheric pressure to ensure the absence of any humidity from the atmosphere inside the cell. The specimen temperature could be decreased by the addition of liquid nitrogen to the Dewar flask. On the other hand, high temperature measurements were taken using normal heaters.

Irradiation

The radiation environment stimulated in these tests is that which a satellite at synch-ronous altitude would encounter. The total fluencies are the averages of the integrated flux over a full solar cycle, including both a solar maximum and different period. In the actual testing, only a fixed number of different particle energies can be used. Protons with seven (0.6, 1.0, 1.5, 2.0, 3.0, 4.0 and 6.0 MeV) and electrons with three energies (6.0, 9.0 and 12.0 MeV) were used. The fluencies at each energy were determined by taking the continuous spectra of space particles and the energy dependencies of the damage rates and combining them to give equivalent fluencies at the test energies (Kalma and Fischer, 1987).

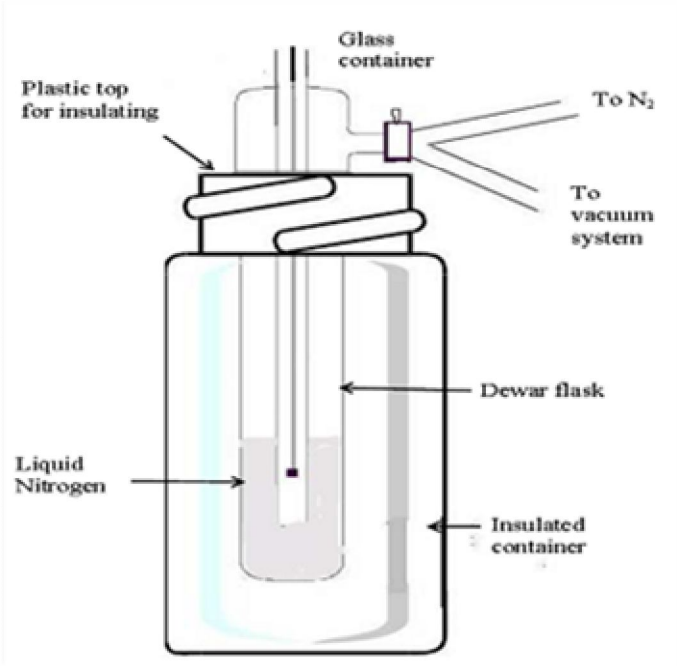

Figure 5. Cooling system used for controlling the samples low temperature levels.

Proton irradiation

Samples were attached to a sample holder of 16 inch Rutherford-Back scattering chamber to receive accelerated protons in the perpendicular direction from a "KFUPM" Tandetron (Al-Juwair et al., 1990). The Tandetron terminal voltage (V) can be controlled within the range from 0.20 to 3.0 MV with a non-stability of the order of ±0.050%. The particle energy is:

$$E = (1 + Qs)V \quad (5)$$

Where, Qs is the charge state.

A high energy switching magnet selects the charge state and directs the beam on the target centre. During irradiation, beam uniformity over the cells holder was obtained by scattering foils (1-mil tantalum and 16.5-mil

polyethylene, for low protons energy up to 3.0 MeV, while 6-mil lead was used for proton energies up to 15 MeV). The thickness necessary was calculated from the theory given by Marion (Marion and Young, 1966). The energy loss was calculated from Janni (nd) and the beam uniformity about 98% was experimentally determined and checked (Marion and Young, 1966).

Electron irradiation

Si-photovoltaic cells with 10 × 5 mm in dimensions have been irradiated at Centre Hospitlier, Lyon Sud, France, with different electron fluencies up to 1.0×10^{13} electron/cm^2, at energies up to 12 MeV.

RESULTS AND DISCUSSION

Temperature effects

The short circuit current and open circuit voltage (Weidong, 2004), for the proposed silicon solar cells with their temperature dependences on were plotted within the temperature range from +300°C down to 160°C. This was carried out in two temperature ranges steps:

1. From room level (30°C) down to -160°C, and
2. From room level (30°C) up to + 300°C.

For both temperature ranges, it was found that the short circuit dependence current on temperature is around: 7.50 µA/°C for the first temperature range, and 5.60 µA/°C for the second temperature range. In this concern, Figure 6a shows the silicon solar cell short circuit current as temperature function in the range from -160°C up to + 300°C, where for the whole temperature range, I_{sc}/°C was shown to be around +/- 6.42 µA/°C. On the other hand, considering the open circuit voltage, and for the two temperature ranges, V_{oc}/°C values of 2.375 and 2.06 mV/°C were reported. From which Figure 6b shows the silicon solar cell open circuit voltage as temperature function in the range from -160°C up to + 300°C, where the dependence V_{oc}/°C was shown to be +/- 1.90 mV/°C. The slope sign depends on the temperature direction relative to the room level.

The study was extended to include the output power dependence of the silicon solar cell on temperature within the pre-determined ranges. Figure 6c shows the silicon solar cell output power as temperature function in the range from -160°C up to + 300°C. The rate of power change, as a function of the temperature range was calculated to be 15.64 µW/°C. For the open circuit voltage and output power, the obtained dependences on temperature were shown to be valid up to 250°C temperature level, where for higher levels, saturation on both parameters was observed.

Practical formulas were deduced for the temperature determination effects on the three parameters of the solar cell, which were given as:

$$V_{out} = V_{ref} [1 -/+ 1.9 \times 10^{-3} (T -/+ 30)]$$
$$I_{sc} = I_{ref} [1 -/+ 6.42 \times 10^{-6} (T -/+ 30)] \quad (6)$$
$$P_{out} = P_{ref} [1 -/+ 15.6 \times 10^{-6} (T -/+ 30)]$$

The solar cells spectral response was investigated as temperature function within the proposed range (Figure 7). It had been shown that the silicon cell sensitivity against light wavelengths ranges approximately from 0.30 µm up to 0.95 µm. The general behavior was shown, and it was found that a small shift on the response curve, either toward lower or upper wavelengths, depending on the temperature variations direction increase or decrease.

Radiation effects

Electron irradiation

The experimental data for the solar cell (I-V) relationship is shown in Figure 8. Room temperature (I-V) characteristics for the samples before and after exposure to different 5.0×10^{12} e/cm^2 electron beams, at 6.0 MeV of energy, 1.0×10^{13} e/cm^2, at 9.0 MeV of energy, and 1.0×10^{13} e/cm^2, at 12.0 MeV of energy, are shown. A pronounced decrease in both the V_{oc} and I_{sc} is shown and consequently the output power appears to be around 80, 67 and 57% of its initial value for the three sample sets, respectively. Finally, Figure 9 shows the spectral response of silicon solar cell before and after exposure to 1.0 MeV electron beams with different fluencies (Zhengyu, 2006; NASA Research Group, 2006).

Protons irradiation

Figure 10a shows that 1.0 MeV proton particles of different fluences ranging from 0.78×10^{15} protons/cm^2 up to 5.78×10^{15} protons/cm^2 produces a serious degradation of the Si-solar cells output characteristics. As an example, at 0.78×10^{15} protons/cm^2 about 50% loss in the open circuit voltage was reported (Srour et al., 2009; Sato et al., 2011). The corresponding loss in the short circuit current is much smaller (around 15%). As consequences of the observed losses are the degradation on the cell output power (Figure 10b). Plotting the maximum power ratios (Pa/Pb) on a log-log scale versus the incident charge (Q); the dependence is found to be linear (Figure 11) and satisfies the following:

$$Pa = Pb.Qi^{-m} \quad (7)$$

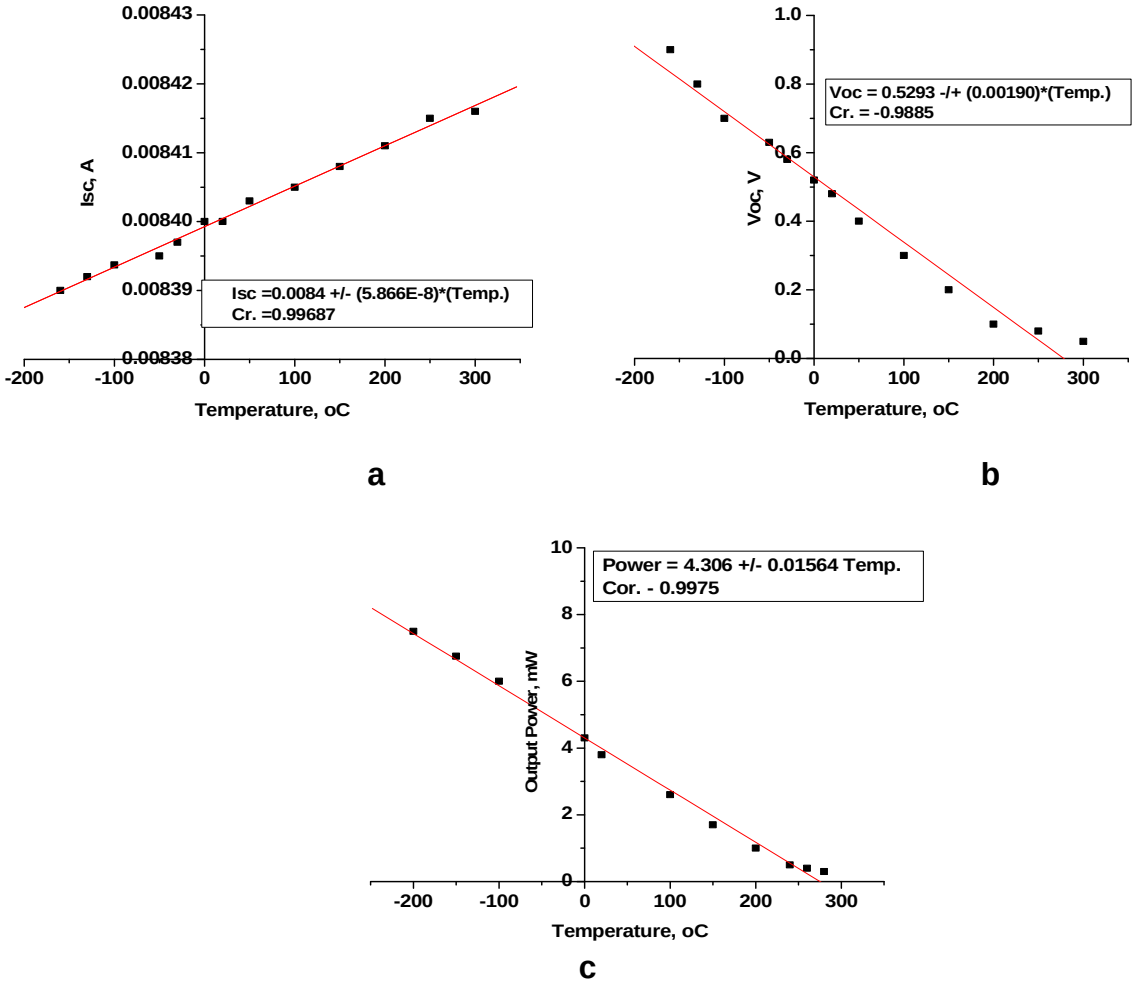

Figure 6. Short circuit current (a), open voltage (b), and output power (c) of Si-solar cell as a function of temperature in the range from -160°C up to + 300°C.

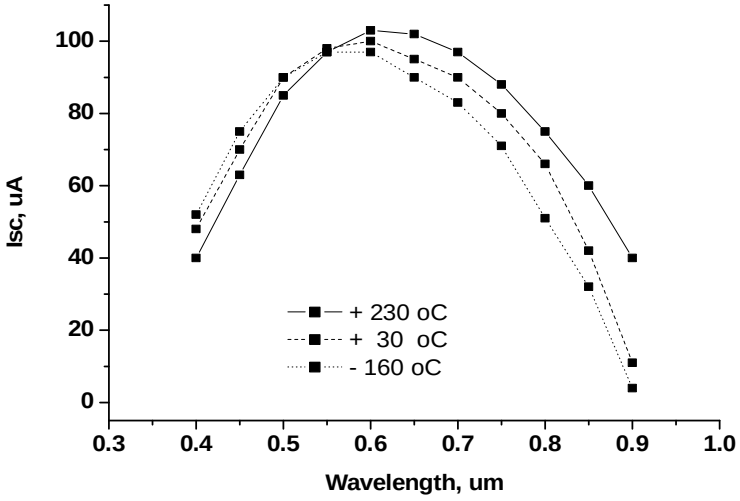

Figure 7. Silicon solar cell spectral response, plotted under the influence of three different temperature levels.

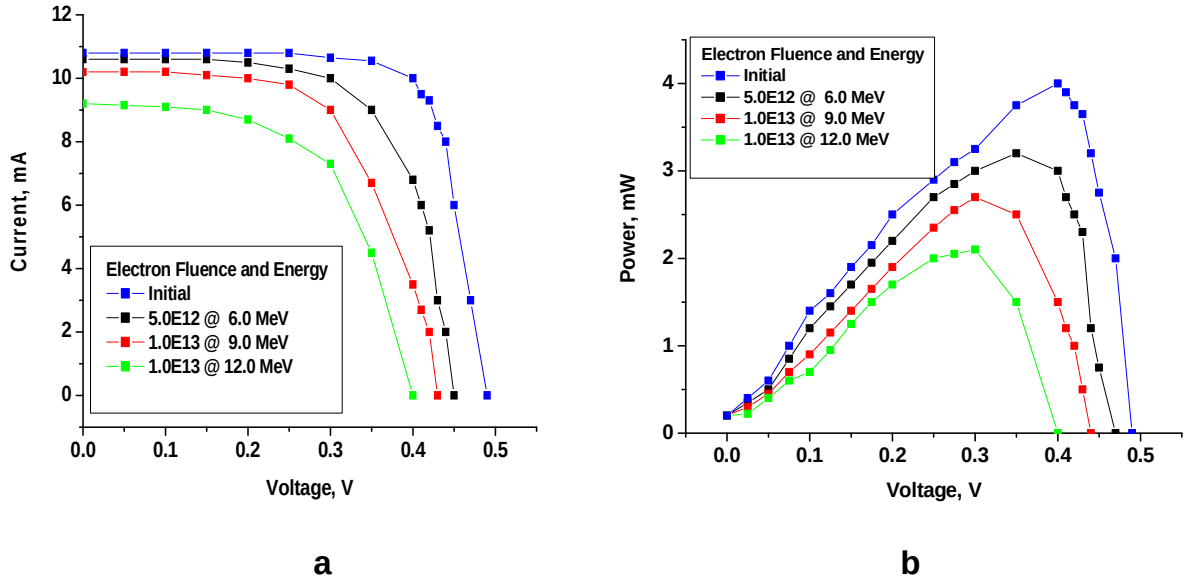

Figure 8. Electron irradiation effects on output (I-V) curves (a), and output power (b).

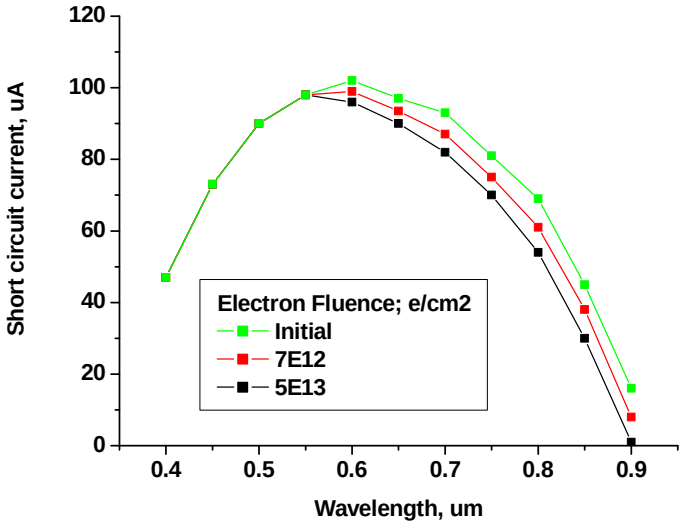

Figure 9. Silicon solar cell spectral response of before and after exposure to 1.0 MeV electron beams with different fluencies.

Where, Pa and Pb are the maximum power (P_{mp}) after and before irradiation respectively, Qi is the incident charge (μC), and m is the curve slope which is shown to be energy dependent (Figure 11a).

The validity of Equation 7 to other experimental geometries should be the subject of further investigations. Finally, Figure 11b shows the silicon solar output parameters damage percentage under 1.0 MeV influence protons with different fluencies.

Figure 12 shows the Si-solar cell relative output parameters dependence on the proton particles energy after irradiation with 0.78×10^{15} p/cm^2. It is clear from the figure that, for low energies up to 3.0 MeV, both the voltage and power ratios increase with the increase in protons energy. For higher energy values, from 3.0 MeV up to 6.0 MeV, the loss rates per particle become almost constant. The observed losses are believed to be due to radiation introduced defect centers which enhance the recombination process and increase the leakage currents. The loss is higher when the defect or trapping

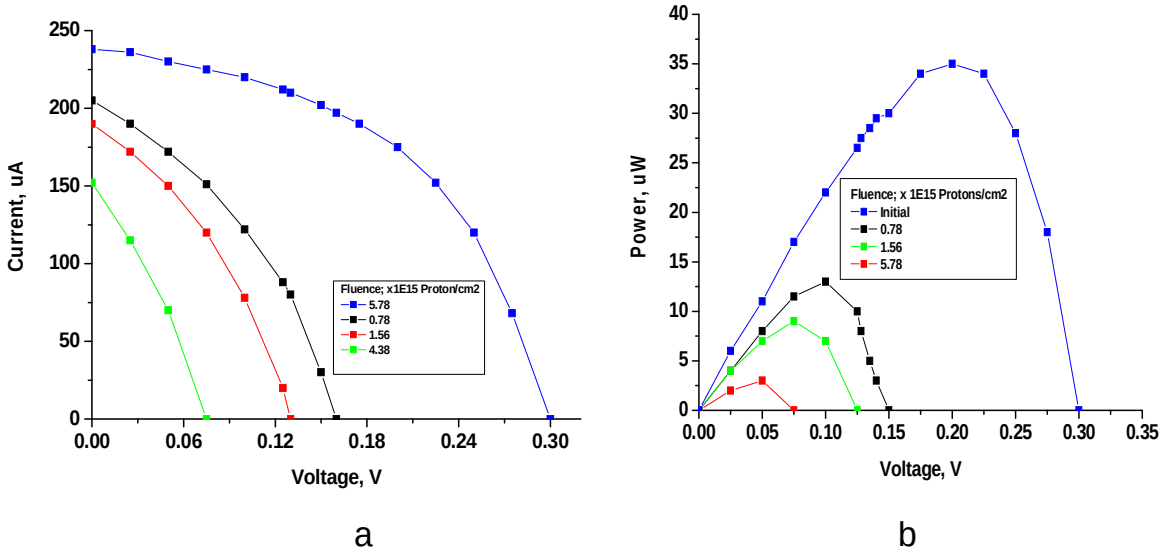

Figure 10. 1.0 MeV protons Influence effects of on current-voltage (a), and power-voltage (b) characteristic curves of silicon solar cells.

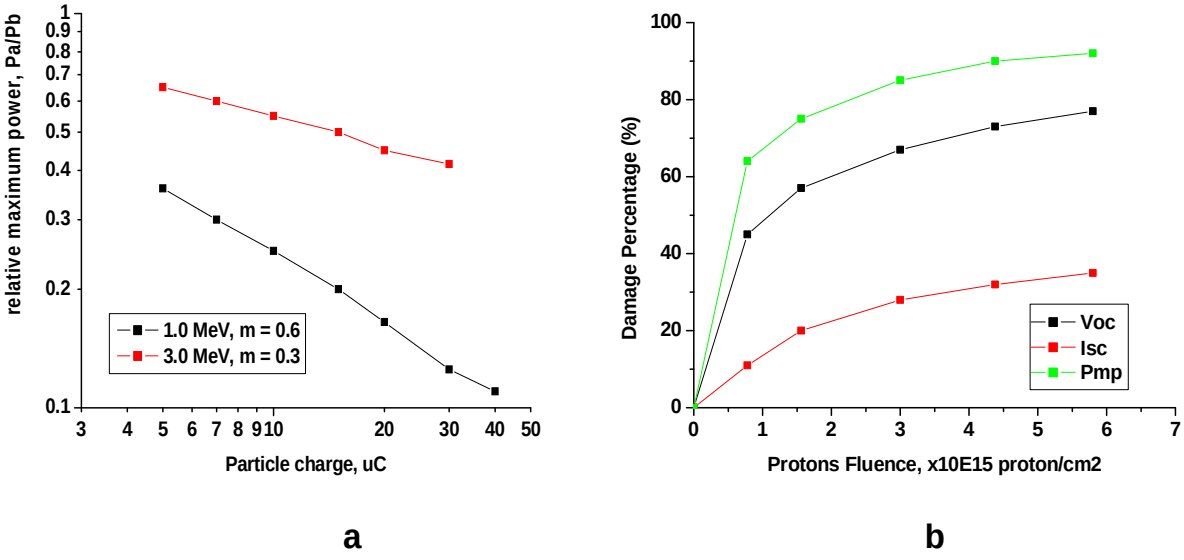

Figure 11. Dependence of relative maximum power ratios on the incident radiation charge (a), and the damage percentage of silicon solar output parameters under the influence of 1.0 MeV protons with different fluencies (b).

centers are closer to pn-junction. Therefore, the PV cell performance after irradiation depends on the defects number introduced (which depends on the radiation fluence), as well as, on their position with respect to the junction (which depends on the particle energy).

Experimental results shown in Figure 13 show that both the forward- (Figure 13a) and reverse- (Figure 13b) currents increase after irradiation with 1.0 MeV proton fluence. The effect is more appreciable at low bias voltage (0.40 V) which may indicate the presence of shallow levels trapping centers near the junction region. This increase in the reverse current will contribute to the reduction observed in the terminal voltage. In the meantime an active recombination process will take place via the radiation induced defect centers, this will result in the minority carriers lifetime degradation and diffusion length, and hence, narrowing of the active region width. Such effect could be realized by capacitance voltage

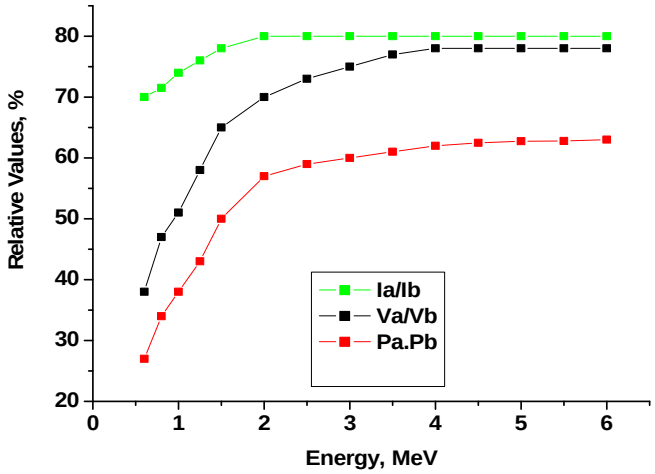

Figure 12. Silicon solar cell relative output parameters dependence on proton particles energy after irradiation with 0.78×10^{15} p/cm^2.

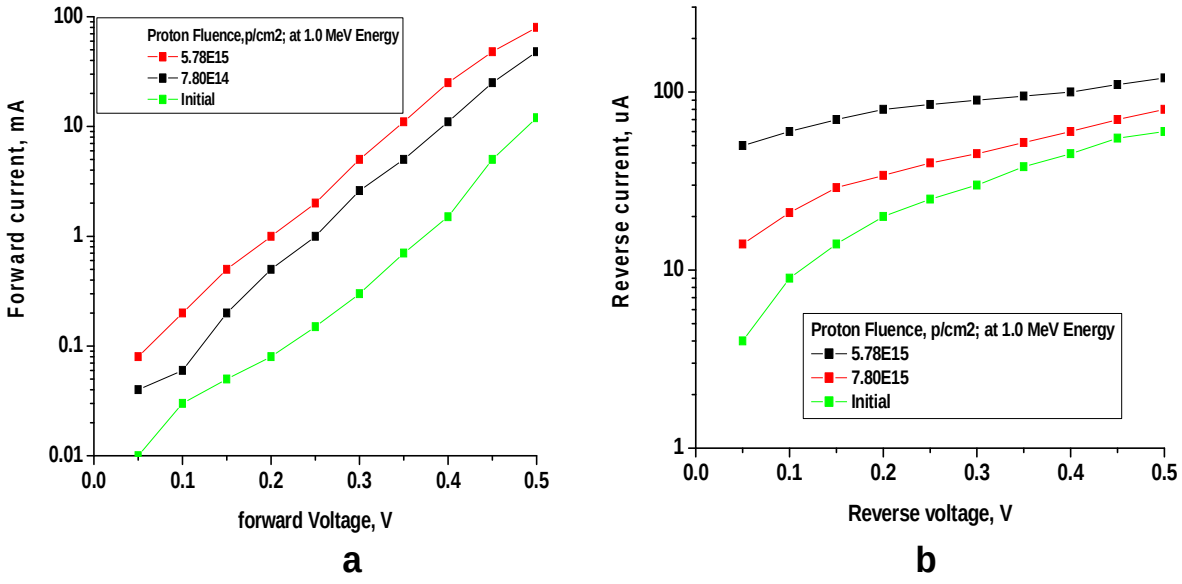

Figure 13. Forward (a) and reverse (b) electrical characteristics of Si-solar cell under the influence of 1.0 MeV protons irradiation.

measurements. However, since the sample capacity was higher than the instrument range, "C-V" measurement was not possible to carry out on these samples. As consequences of these effects are the output power degradation of the irradiated solar cell.

The PV cell samples output power is plotted versus the terminal voltage in Figure 14, after irradiation with 7.8×10^{15} p/cm^2 at different protons energy of 0.6, 1.0, 1.5, 2.0 and 4.0 MeV, respectively. The maximum power values (P_{mp}) decrease with the decrease in particle energy associated with lower terminal voltages. The damage rate is higher at lower energies down to 0.6 MeV. The results shown in Figure 14 confirm that Si-PV cell power degradation by proton irradiation is energy dependent. The damage rate is higher when the particles are stopped closer to the depletion region. Irradiation with relatively higher energy non-penetrating particles can produce similar defect centers but since they are localized at more distances from the junction, their damage effect will be lower.

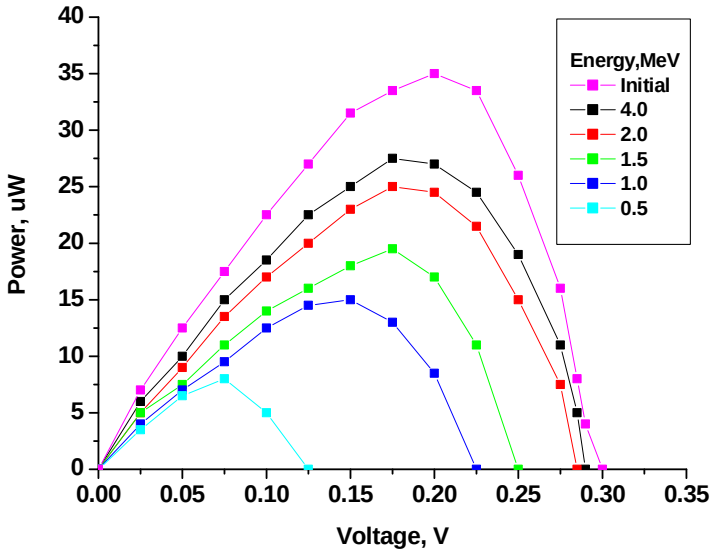

Figure 14. Silicon solar cell output power of irradiated with proton fluence of 0.78×10^{15} p/cm^2, at different energy levels.

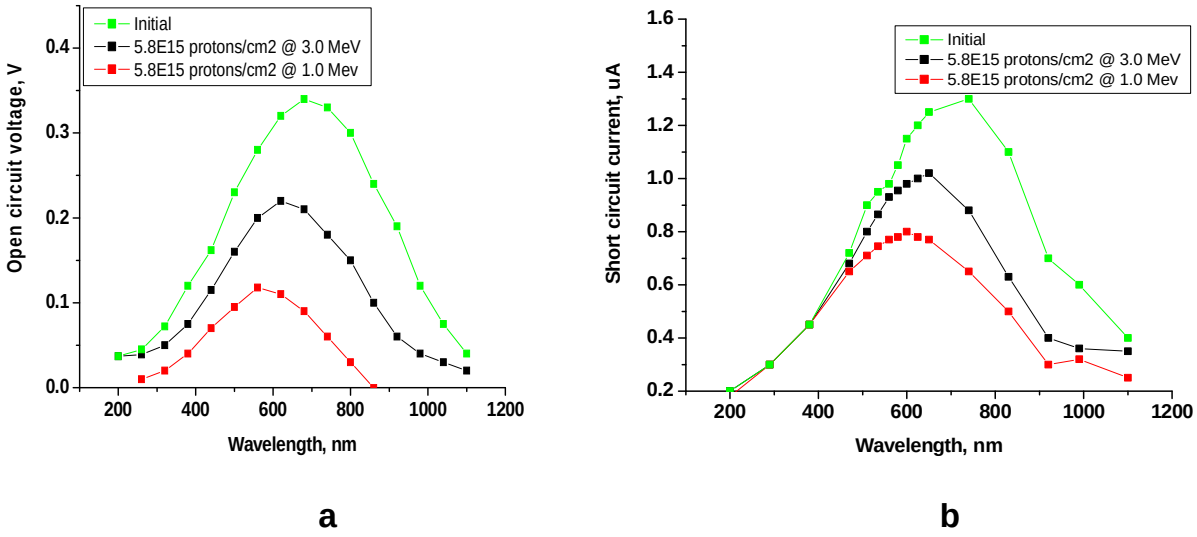

Figure 15. Open circuit voltage (a) -, and short circuit current (b) - spectral responses before and after exposure to 5.8×10^{15} protons/cm^2 at two different energy levels of 1.0 and 3.0 MeV.

Finally, the proton exposure effect on the spectral response of the silicon solar cells was investigated. In this concern, Figure 15 shows the experimental spectral open circuit voltage responses (Figure 15a), and short circuit current (Figure 15b), both plotted as a functions of the wavelength in the range from 200 nm up to 1100 nm, before and after exposure to 5.8×10^{15} protons/cm^2 at two different energy levels of 1.0 and 3.0 MeV. It is clearly observed that the radiation damage manifests itself as a decreased red-infrared response of the cell, that is, the current and voltage, due to the long wavelength light absorption were reduced. Losses in short circuit current started at 500 nm and increased at longer wavelengths to reach its maximum at about 650 to 700 nm beyond which appreciable losses were in the infrared band. Losses in terminal voltage occurred even in the UV range and increased at longer wavelengths having a peak loss at about 700 nm. Both the current and voltage responses confirm that the radiation degree damage by protons is energy dependent.

CONCLUSION

From the study, experimental results, theoretical analysis, and interpretation, it is clearly shown that for the temperature range from +300°C to -160°C, the short circuit current of the Si-solar cells was shown to be un-sensitive function of temperature. The main variation was observed to be due to open circuit voltage, and consequently, the cell output power. On the other hand, electron-and proton-irradiation effects on characteristics of photo-voltaic cells were investigated. Only permanent damage is observed and serious degradation occurred in both open circuit voltage and short circuit current and consequently reduces the output power of the cell. The effects were shown to be a function of both fluence and energy of the incident radiation. Finally, it is clearly shown that silicon solar cells are sensitive to both temperature and nuclear radiation, so cautions should be considered.

REFERENCES

Abdel Basit W, El-Ghanam S, Abd El–Maksood AM, Soliman FAS, **2013**. Performance of shunt voltage regulators based on Zener diodes at cryogenic temperatures. Phys Sci Res Int, 1(2):16-24.

Adams L, Daly EJ, Harboe-Sorensen R, Holmes-Siedle AG, Ward AK, Bull RA, **1991**. Measurement of SEU and total dose in geostationary orbit under normal and solar flare conditions. IEEE Trans Nuclear Sci, 38(6):1686–1692.

Al-Juwair HA, Al-Kofahi, MM, Hallak AB, Rajeh M, **1990**. A 3.0 MV Tandetron facility at KFUPM. Nucl Inst Meth Phys Res, B-50:474-477.

Cattell C, **2008**. Discovery of very large amplitude whistler-mode waves in earth's radiation belts. Geophys Res Lett, 35(1), L01105, doi:10.1029/2007GL032009.

Earth's *Radiation Belts*: A Tutorial - ACD. www.acd.ucar.edu/Events/Meetings/.../Baker.pdf.

El-Ghanam SMR, **Abdel Basit** W, **2011**. Performance of electronic switching circuits based on bipolar power transistors at low temperature. Cryogenics, 51(3):117–123.

Gordon I, **2015**. Solar Energy Materials and Solar Cells. EMRS 2014 Spring Meeting-Advanced Materials and Characterization Techniques for Solar Cells II, Vol. 135, pp. 8-16.

Holmes-Siedle A, **Adams** L, **2002**. Handbook of Radiation Effects (2nd Ed.). Oxford; New York: Oxford University Press.

Janni JF, **nd**. Calculations of energy loss, scattering and probability of inelastic nuclear collisions for 0.10 to 1000 MeV protons. AFWL-TR-1966.

Johnson MH, **Kierein** J, **1992**. Combined release and radiation effects satellite (CRRES): Spacecraft and mission. J Spacecraft Rockets, 29(4):556-563.

Kalma AH, **Fischer** CJ, **1987**. 4π space radiation of solar cell. IEEE Trans Nucl Sci, 23(6):1789-1795.

Marion J, **Young** FC, **1966**. Nuclear reaction analysis and tables. North-Holland Publishing Company, Amestrdam, 1966.65-150.

Marzouk M, **Soliman** FAS, **1987**. Computer analysis of radiation effects on Si - Solar cells. 12th Intr. Cong., for Statistics, Computer Sci., and Social Research, Cairo, Egypt, 28 March – 2 April.

NASA Research Group, **2006**. NASA investigates proton radiation effects on silicon solar cells Johnson NASA Space Radiation Laboratory at Brookhaven National Laboratory, Upton, N.Y., Aug. 2006.

NASA, **nd**. Radiation Belt Around Earth Discovered By NASA's Van Allen Space Probes. HUFF Post Science, www.huffingtonpost.com/.../new-radiation-belt-earth.

Novikov LS, **2008**. Space radiation effects simulation methods. Lomonosov Moscow State Univ., SINP MSU Preprint - 9 / 722, 2008. Skobeltsyn Instit. of Nucl. Physics.

Owen T, Mahaffy P, Niemann HB, Atreya S, Donahue T, Bar-Nun A, de Pater I, **1999**. A low-temperature origin for the planetesimals that formed Jupiter. Nature, 402:269-270.

Proton Belt, nd. **www.astrogle.com/discus/index.php?topic=1092.0**.

Santina G, Nieminen P, Evans H, Dalya E, Lei F, Truscott PR, Dyer CS, Quaghebeur B, Heynderickx D, **2003**. New Geant4 based simulation tools for space radiation shielding and effects analysis. Nuclear Physics B - Proceedings Supplements, 125:69-74.

Sargent-Welch, nd. https://www.sargentwelch.com/store/jump/sku/...03EA/SOLAR+CELL.

Sato S, Sai H, Ohshima T, Imaizumi M, Shimazaki K, Kondo M, **2011**. Electron and proton irradiation effects on substrate-type amorphous silicon solar cells. Photovoltaic Specialists Conference (PVSC), 37th IEEE, Seattle, WA, USA, pp. 1615 – 1619, 19-24 June 2011.

Shprits YY, Elkington SR, Meredith NP, Subbotin DA, **2008**. Review of modeling of losses and sources of relativistic electrons in the outer radiation belt. J Atmospheric Solar-Terrestrial Phys, 70(14):1679–1713.

Silverman EM, **1995**. Space environmental effects on spacecraft: LEO materials selection guide, part 2", Progress Report, TRW, Inc., Redondo Beach, CA. Space and Electronics Group.

Soliman FAS, **1988**. Theoretical analysis of radiation effects on power diode characteristics. Isotopenpraxis, 24(9):349-355.

Srour JR, Palko JW, Lo DH, Liu SH, Mueller RL, Nocerino JC, **2009**. Radiation effects and annealing studies on amorphous silicon solar cells. IEEE Trans on Nucl Sci., 56(6):3300-3306.

Stassinopoulos EG, **2003**. The space radiation environment for electronics. Proceedings of the IEEE, 76(11):1423-1442.

Torchynska TV, **2004**. High efficiency solar cells for space applications. Superficies Vacio, 17(3):21-25.

Weidong X, **2004**. A novel modeling method for photovoltaic cells. Power Electronics Specialists Conference, 20-25 June 2004. PESC 04, 2004 IEEE 35th Annual Conf., 3:1950-1956.

Zhengyu HU, **2006**. Radiation effects of protons and electrons on backfield silicon solar cells. Research-Gate, 07/2006; DOI:10.1007-4020-4039-8_1, pp. 1-8.

Citation: El-Ghanam SM, Abd El-Basit W, Soliman FAS, 2015. Simulating the operation of silicon photovoltaic cells at outer space environments. Adv Sci Tech Res, 2(3): 42-53.